Lu *et al. Chem. Biol. Technol. Agric.* (2023) 10:60
https://doi.org/10.1186/s40538-023-00386-8

Chemical and Biological Technologies in Agriculture

RESEARCH

Open Access

Mathematical modeling of modified atmosphere package/LDPE film combination and its application to design breathing cylinders for extending the shelf life of green asparagus

Wen-Chien Lu[1†], Yu-Tsung Cheng[2,3†], Chien-Jung Lai[4], Been-Huang Chiang[5], Ping-Hsiu Huang[6*] and Po-Hsien Li[3*]

Abstract

Background The O_2 levels in food packaging systems play an essential role in the deterioration of food quality and shelf life. Modified atmosphere packaging (MAP) supports the storage of fresh and processed foods by inhibiting chemical and physical changes while reducing the deterioration caused by microorganisms.

Materials and methods This study established and validated the equations for the relationship between MAP formulation reagents, asparagus respiration, permeability of packaging film, and rates of O_2 and CO_2 mass transfer in which different interactions occur and affect each other.

Results The resulting atmosphere of packaging was determined to be the key to achieving the MAP benefits. The active MAP formulations developed in this study were combined with very-low-density polyethylene films to store green asparagus spears. During storage, the combined films effectively maintained the firmness of green asparagus spears, fiber, and vitamin C content, and outperformed the passive MAP and control groups. The above results confirm all the equations in the passive and active MAP systems established in this study.

Conclusions Hence, maintaining the asparagus quality with an active MAP treatment will reduce economic loss and possibly provide new insights into applying active MAP retail packages to preserve fruits and vegetables in post-harvest shelf life.

Keywords Modified atmosphere packaging (MAP), Retail packages, Asparagus spears, Respiration rate, Post-harvest shelf life

†Wen-Chien Lu and Yu-Tsung Cheng contributed equally to this work

*Correspondence:
Ping-Hsiu Huang
hugh0530@gmail.com
Po-Hsien Li
pohsien0105@pu.edu.tw
Full list of author information is available at the end of the article

Graphical Abstract

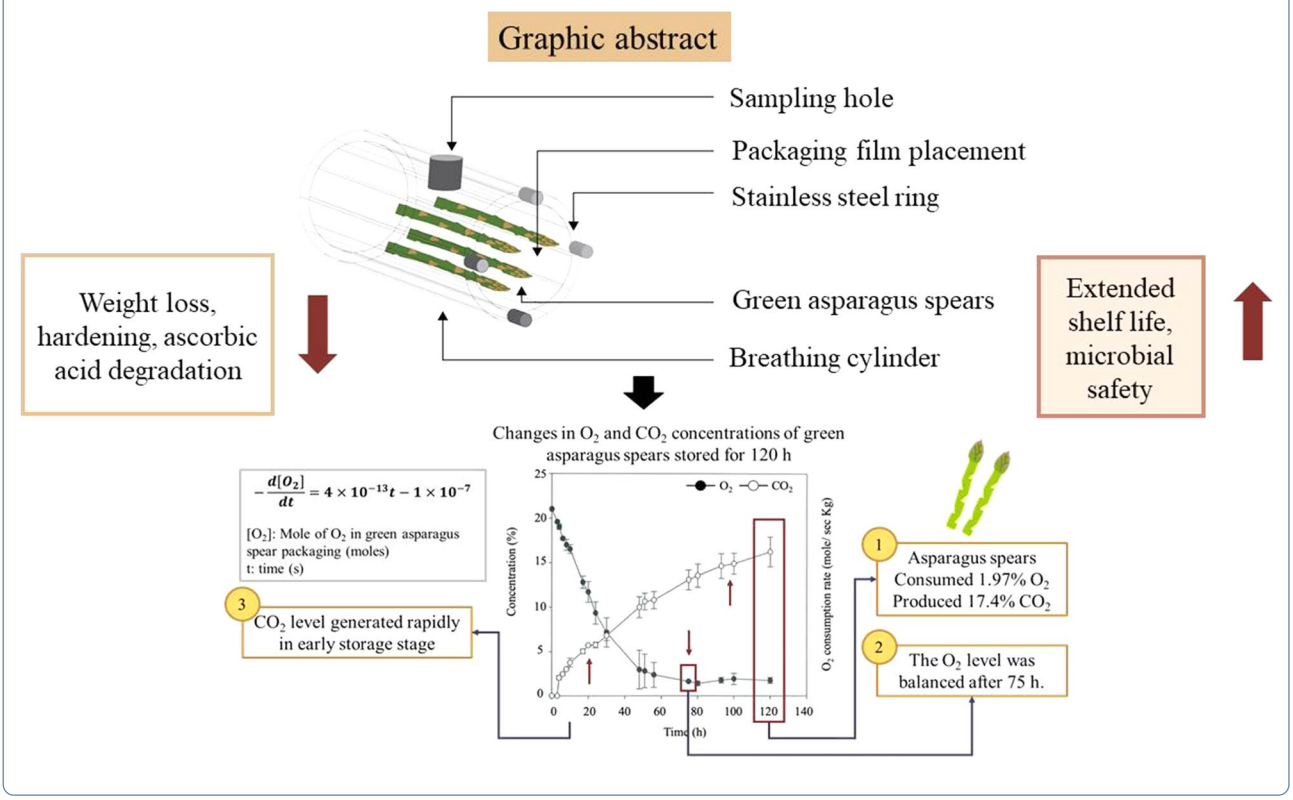

Introduction

Asparagus (*Asparagus officinalis* L.) is a perennial edible crop cultivated in various climatic regions worldwide [36, 41]. Consumers favor asparagus spears because of their low calorie content, high fiber content, unique flavor (originating from sulfur-containing compounds), and bioactive substances (vitamins, fructose, flavonoids, and steroidal saponins), which characterize most of the health benefits of their consumption [4, 14, 30, 38, 40, 41]. Global asparagus production grew at an average annual rate of 4.14%, from 1.23 to 8.45 million tons (1971–2020) [34], and is estimated to reach 10 million metric tons by 2027 [24]. In general, asparagus spears are highly perishable and have a shelf life of 3–7 days at ambient temperatures; thus, they deteriorate rapidly after harvest [23, 36] and under refrigerated conditions for approximately 12–21 days [1, 30]. Certain foods, such as juice, tea, canned food, and fermentation products, are processed, and the same procedure is applied to fresh asparagus spears to prevent deterioration due to lignification; however, the procedure has a significant effect on the sensory attributes and chemical composition of asparagus [28, 40, 43]. Most consumers in the global market prefer fresh or whole asparagus spears [1]. The worldwide market share of fresh asparagus is 74%, followed by canned and frozen asparagus at 26%. Therefore, more ways to extend the shelf life of asparagus should be explored to meet the consumption tendency.

Several post-harvest treatments have been applied to asparagus, the most widely used is modified atmosphere packaging (MAP) or its combination with other methods (hypobaric storage, ultraviolet C, ozone, hot water, salicylic acid, drying, and chitosan coating) [16, 17, 20, 26, 30, 36]. The public has recognized this technology for its advantage of using only the atmosphere and natural components (O_2, CO_2, and N_2) without creating toxic residues [3, 16]. Combined with refrigeration at 2 °C, MAP reduced weight loss, hardening, and ascorbic acid degradation, improving microbiological safety and extending the shelf life of green asparagus spears [1, 30]. However, each fresh product responds differently to MAP conditions significantly when the O_2 concentration decreases below the critical threshold required to maintain anaerobic respiration and fermentation, which results in off-flavors [18, 42]. The occurrence or accumulation of high CO_2 concentrations may negatively affect the quality of food products [16]. Moreover, the effects of customization of atmospheric conditions on specific agricultural

products must be applied, and imminent risks from incorrect conditions should be avoided. The equations in this study included those for the reaction rate of MAP reagents, O_2 and CO_2 mass transfer rate, packaging film permeability, and respiration rates [16, 18]. This study aimed to construct a mass balance equation for the O_2 consumed and CO_2 produced in the packaging system to simulate the changes in O_2 and CO_2 concentrations in green asparagus with active MAP during the storage period. In addition, the film permeability and respiration rate equation for green asparagus were used to simulate the changes in O_2 and CO_2 concentrations with passive MAP. The internal composition of the packaging atmosphere can be controlled to extend the shelf life of products. This information is crucial to extend the shelf life of asparagus. A proactive approach to asparagus quality maintenance will greatly interest producers because it will increase their economic returns while meeting environmental challenges.

Materials and methods

Materials

Fresh green asparagus with appropriate maturity was harvested randomly from a local farm (Changhua County, Taiwan), followed by washing and cleaning in the laboratory. Green asparagus with over 80% green appearance and intact shape was immediately classified and selected as samples. Asparagus spears were cut from the tip of the asparagus below an 18 cm section (diameter: 10–15 mm), soaked in 5 ℃ sodium hypochlorite solution (200 ppm), precooled for 2 h, and randomly packed into groups. The packaging and storage of green asparagus spears are described in Sect. 2.7. Sodium ascorbate was purchased from Sigma-Aldrich (Merck KGaA, Darmstadt, Germany). Sodium carbonate-10-hydrate and ferrous sulfate-7-hydrate were purchased from Riedel-de Haën (Honeywell International Inc., Charlotte, NC, USA). Calcium chloride was purchased from Wako Pure Chemical Industries Ltd. (Osaka, Japan). The reagent composition of MAP formulations consisted of sodium ascorbate (5.03 g), sodium carbonate (21.78 g), ferrous sulfate (13.40 g), and calcium chloride (5.03 g). Sodium carbonate, ferrous sulfate, and calcium oxide were milled at 5 °C. Sodium carbonate was passed through a 60–100-mesh sieve, and calcium chloride and ferrous sulfate were sieved through a 140–270-mesh sieve. The four formulations were mixed in PE zip-lock bags (85×60 mm^2) in a cold room with N_2 at 5 °C. The formulations were reacted in a closed system (285 mL) at 5 °C for 48 h to maintain an O_2 content of 6.5% and a CO_2 content of 15.5%.

Determination of reaction rate coefficient

Sodium ascorbate oxidation rate constant

Sodium ascorbate ($C_6H_8O_6$) dissociates to ascorbate ($C_6H_7O_6^-$) in solution and continuously reacts with O^- molecules to form $C_6H_6O_6^-$. The sodium ascorbate oxidation rate constant calculation was modified according to the method described by Khamespanah et al. [13]. In brief, at pH 7.0, phosphoric acid buffer solution was prepared in 500 mL glass serum bottles covered with a layer of aluminum foil to insulate the bottles from light. The solutions were immersed in a constant-temperature bath at 5 °C and 25 °C. The value of dissolved O_2 in the solution was detected with a dissolved O_2 electrode (Model 52,200,117, Mettler Toledo Co., Columbus, OH, US) by continuously filling the phosphate-buffered saline bottle with air using a pump and ventilating until the dissolved O_2 value displayed by the electrode reached a stable level. It is worth mentioning that the saturated dissolution of O_2 at 5 °C was 8.9 mg/L. Next, the air supply was stopped, and sodium ascorbate with a starting reaction concentration of 4×10^3 M was added to initiate the reaction. The reaction time was 120 min. An interval of 5 min was used as the sampling point, and a 3 mL sample was obtained each time. The absorbance values were measured using a spectrophotometer (HITACHI-1100, Tokyo, Japan) at a wavelength of 266 nm, and a standard curve was used to calculate the concentration of $C_6H_7O_6^-$. This step was performed in triplicates. By analyzing the degradation rate of ascorbic acid over time and the $C_6H_7O_6^-$ concentration, the following equation shows the reaction rate:

$$\text{Reaction rate} = -\,\mathrm{d}[HA^-]/\mathrm{dt} = K_1 \times [HA^-] \times [O_2]^{1/2}, \quad (1)$$

with $[HA^-]$: ascorbic acid concentration.

In case, $t = 0$. $[HA^-] = 4 \times 10^{-5}$ M; $[O_2] = 2.78 \times 10^{-4}$ M.

The mechanism of the ascorbic acid reaction showed that for each mole of ascorbic acid consumed, 1/2 mol of oxygen was consumed. Therefore, the rate constant (K_1) was obtained from the rate equation by calculating the dissolved oxygen concentration and slope value at different time points with the ascorbate concentration.

Oxidation rate constant of ferrous sulfate

As reported by Baldwin and Van Weert [2] and Jones et al. [12], the ferrous ion autoxidation reaction was performed with appropriate modifications. The reaction tank was filled with 3 L of deionized water at 5 ℃ and 25 ℃ and pumped with air. The dissolved O_2 level was measured using a dissolved oxygen meter (Model D-25, Horiba Ltd., Kyoto, Japan), which stopped ventilation when

the dissolved O_2 reached a stable level. Next, sodium carbonate was added with up to 2×10^{-2} eq/L equivalent concentration of alkali, followed by a solution filled with CO_2 gas to maintain the solution system at pH 7.0. Ferrous sulfate was immediately added at a concentration of 0.025 g/L. After the 120 min reaction period, 1 mL of the sample was withdrawn every 5 min, and the ferrous ion concentration was promptly analyzed. Experiments were performed in triplicate. The ferrous ion concentration analysis was performed as described by Serra-Mora et al. [32], with some modifications. The sample was added with 2 mL O-phenanthroline monohydrate, which is specific for the reaction of ferrous ions, rapidly leading to a pink reaction. The absorbance was measured at a wavelength of 510 nm, followed by a standard curve to calculate the concentration of ferrous ions. The reaction rate equation is as follows:

$$\text{Reaction rate} = -\,d[Fe^{2+}]/dt = K_2 \times [Fe^{2+}] \times [O_2]^{1/4}. \quad (2)$$

In case, t=0, $[Fe^{2+}]=8\times10^{-5}$ M, and $[O_2]=2.78\times10^{-4}$ M. The dissolved oxygen concentration depends on the response mechanism of ascorbic acid. Therefore, the ferrous ion concentration at different time points correlated with the dissolved oxygen concentration. This indicates that for each 1 mol of ferrous ions consumed, 1/4 mol of oxygen was consumed simultaneously. Hence, the rate constant (K) was calculated using the rate equation to calculate the dissolved oxygen concentrations and slopes at different time points.

Determination of the coefficient of mass transfer

Determination of oxygen mass transfer coefficient (KL)

The equations described by Lee [16] were modified for derivation. The mass transfer rate of O_2 diffusion from the gas to the liquid phase was determined by gassing out N_2 to reduce the dissolved O_2 level in the solution. The validation method was performed using a 1 L glass serum bottle containing deionized water. The bottle was placed in a refrigerator at 5 °C with continuous N_2 ventilation, and dissolved O_2 was detected until horizontal fixation. The bottle cap was tightly locked and placed in a refrigerator at 5 °C until ready for use. Every 30 min, 200 mL of deionized water was sampled in a 500 mL beaker. The dissolved O_2 electrode was immediately placed in it, with the top end dipping 7 mm below the water surface before starting observation. The change in the dissolved O_2 level was recorded for 5 h. The equation for the mass transfer rate of O_2 is as follows:

$$d[C_L]/dt = K_L \times \left(C_L^* - C_L\right). \quad (3)$$

In case, $t=0$, $C_L=C_0$. The following equation was obtained by integration.

$$\ln\left(C_L^* - C_L\right)/\left(C_L^* - C_0\right) = -K_L \times (t - t_0). \quad (4)$$

The slope K_L can be obtained by plotting ln (C^*_L- C_L)/ (C^*_L—C_0) on (t—t0).

C_L (t) is the measured dissolved oxygen level measured in the solution at any time.

C_0 is the initial concentration of the dissolved O_2 in the solution.

C^*_L indicates the level of saturated dissolved O_2 in the solution.

Determination of CO_2 mass transfer rate constant (K_g)

The equations described by Schmitz [29] and Demirel [9] have been modified. The rate of CO_2 mass transfer from the liquid phase to the gas phase was determined using the mass transfer rate constant of CO_2. Distilled water 800 mL was added to a 1192 mL triangular cylindrical flask and refrigerated at 5 °C for 1 h. CO_2 gas was pumped into the triangular flask for 2 h, which was closed with a stopper and rested for 3 h. By opening the stopper, air convection in the headspace of the flask was forced out, thereby exchanging the air inside and outside the flask. The flask was then closed with a stopper, followed by a closed gas syringe for sampling and analysis of the gas composition in the flask. Subsequently, samples were obtained once every 1 h. Finally, the five points were analyzed in triplicate. The CO_2 mass transfer rate coefficient was calculated.

Gas-phase mass transfer.

$$d[C_g]/dt = K_g \times \left(C_g^* - C_g\right). \quad (5)$$

In the case of $t=0$ and $C_g=C_0$, the following equation is obtained by integration:

$$\ln\left(C_g^* - C_g\right)/\left(C_g^* - C_0\right) = -K_g \times (t - t_0). \quad (6)$$

The slope, K_g, can be obtained by plotting (t—t0) and ln (C^*_L- C_L)/ (C^*_L—C_0).

C^*_g is the vapor-phase saturation concentration of CO_2 and is expressed as $H\times x_A$.

H means Henry's constant at 20 °C (CO_2: 0.142; O_2: 4.01).

x_A is the mole fraction of CO_2 in the solution.

C_g is the CO_2 concentration of the gas phase (headspace).

C_o is the initial CO_2 concentration.

Determination of saturated solubility

Sodium carbonate

The analysis was performed using a modification described by Rajesh et al. [27]. At room temperature, 5 g of sodium carbonate was obtained and dissolved in 10 mL of distilled water. The mixture was thoroughly stirred to achieve

complete dissolution. Subsequently, the solution was allowed to stand in a refrigerator at 5 °C, and sodium carbonate crystals precipitated. The crystallized sodium carbonate was filtered using Whatman No.1 filter paper, dried at 45 °C, weighed, and calculated using the following equation:

$$\text{Saturation solubility of sodium carbonate (S)} = (W_0 - W_1)/W_0 \times 100, \quad (7)$$

where W_0 means 5 g sodium carbonate and W_1 is the weight of crystallized sodium carbonate.

Sodium ascorbate

The method was performed following the work of Serpa et al. [31] with modifications. A total of 10 mL of distilled water solution was added to a beaker and an excess amount of sodium ascorbate solids was added in a cooler with the temperature controlled at 5 °C until complete stirring. Every 10 min, a 1.5 mL sample was collected and centrifuged at 6000 rpm for 3 min. The supernatant was withdrawn, and the centrifugation was repeated once. 100,000 folds diluted the clarified solution, the absorbance was measured at 266 nm, and the concentration was calculated using standard curves. The measured concentration was the saturation solubility of sodium ascorbate at 5 °C until the concentration no longer changed over time.

Ferrous sulfate

In the same procedure as in Sect. 2.3.3.2, with the only difference of dilution to 100,000 folds, a 1 mL sample was obtained and added to 2 mL of 0.2% *O*-phenanthroline monohydrate solution for the color rendering reaction. Absorbance was measured at 510 nm. The concentration of ferrous ions was calculated using a standard curve representing the saturated solubility of ferrous sulfate at 5 °C.

Determination of membrane film gas transmission rate

The method used was modified according to the work of Tian et al. [36]. Two identical aluminum trays (inner diameter: 12.87 cm, depth: 3.02 cm, volume: approximately 393 mL) with an inner diameter of 13.3 cm, a width of 0.4 cm, a depth of 0.2 cm, a circular groove, and where an *O*-ring that can be placed were used. Each aluminum tray had two ventilation valves, and the extraction hole was plugged with a silicone plug with a diameter of 6 mm. The *O*-ring and groove were coated with Vaseline, and the sample film was clamped between the two aluminum trays with screws to make the entire device airtight. In a cold room at 5 °C, N_2 flowed into the upper aluminum chamber (chamber A) and the sample gas (O_2 and CO_2) into the lower aluminum chamber (chamber B). The flow rate was 25 mL/min with a pressure of 1 atm. The gas was then inserted for 2–3 h to allow complete air replacement in the tray by N_2 and for sample collection. Initially, both valves of chamber A were closed. In contrast, chamber B was continuously filled with gas for the measurement. A sample was obtained at regular intervals, and the gas (0.5 mL) in chamber A was extracted using a closed gas syringe and analyzed using gas chromatography (GC) (Model GC320, Gasukuro Kogyo Co., Tokyo, Japan). When the ventilation valve was closed at the zero point, sampling was performed once every 2 h for 10 h (CO_2 gas transmission rate) to 20 h (O_2 transmission rate) to determine the changes in gas concentration. The formula for the gas transmission rate of packaging films according to Fick's 1st law is as follows [7, 16]:

$$dn/Adt = P\,(dC/dX), \quad (8)$$

P: Gas transmission coefficient (cc-mil/m^2- 24 h); A: Film footprint (m^2); X: Film thickness (mils, 1 mil = 1/1000 in or 25.4 μm); dn: The amount of change for the sample gas concentration; dC: The difference in concentration of the sample gas at both ends of the film.

Gas content analysis

The detection was performed following the methods of Langham [15] and Sergio et al. [30] with minor modifications. A 0.5 mL gas sample was randomly drawn from the package's headspace and analyzed for O_2 and CO_2 in the container using GC (Trace 1310, Thermo Fisher Scientific Inc., Waltham, MA). A molecular sieve (5A column, 6 ft × 1/8") and thermal conductivity detector were used. Helium was used as the carrier gas at 40 mL/min flow rate. The inlet and detector temperatures were set to T 30 °C. The oven temperature was controlled during the analysis using a temperature-rise program initially set at 30 °C. The standard curves were analyzed using the following gas mixtures with known concentrations (%): (1) 39% helium, 40% CO_2, and 21% O_2; (2) 70% helium, 20% CO_2, and 10% O_2; (3) 80% helium, 15% CO_2, and 5% O_2; and (4) 98% helium, 1% CO_2, and 1% O_2. The peak areas and concentrations were regressed to obtain the O_2 and CO_2 content standard curves. A GC analysis was performed to determine the relative reaction factor (RRF). Subsequently, each sample's O_2 (or CO_2) content was determined from the peak area, and the RRF values were obtained from GC analysis.

Design of the breathing cylinder and the respiration rate of green asparagus spears

The breathing cylinder with a glass cylinder (140 mm outer diameter, 133 mm inner diameter, and 180 mm height) had a total volume of 2920 cm^3 (Fig. 1), with two stainless-steel rings at each end. One was fixed on a glass

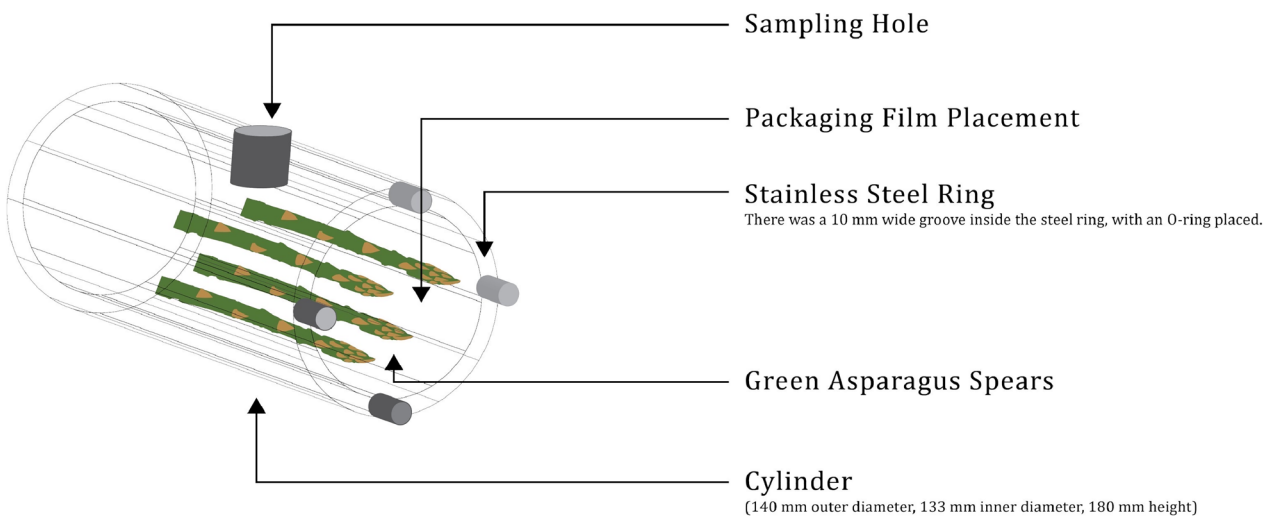

Fig. 1 Schematic of the breathing cylinder

cylinder with a 10-mm-wide groove inside the steel ring and an *O*-ring was placed. The other ring has four screws attached to a glass cylinder. The sample films were fixed between two circles and set with an *O*-ring. A sampling hole was made in the cylinder and secured using a silicone pad. The method described by Li and Zhang [18] was used to determine the respiration rate of green asparagus spears, with modifications as appropriate. A total of 800 g of green asparagus spears (pre-treatment as described in "Materials" section) was wiped, drained, and packed into the above glass breathing cylinder (total volume of 2920 cm^3), with a residual volume of 2086 cm^3 for 120 h of observation and periodic analysis of the atmospheric composition in the cylinder.

Film and MAP effects on storage of green asparagus spears

Passive and active MAP

The film used in this study was a very-low-density polyethylene (VLDPE) film with a thickness of 60 μm, which was cut to 165 × 165 mm^2. Then, 500 g of green asparagus spears (as described in "Materials" section) was weighed and added to the MAP (formulations described above in "Materials" section) with the film clamped in the steel ring on both sides, forming a food packaging system with atmospheric transmission. The packaging was refrigerated at 5 °C and sampling was performed each day during the initial storage period. After 10 days, sampling was conducted every 3 days to analyze the gas composition in the packaging by GC; the entire storage period was 20 days.

Practical application of active MAP

PE zipper bags (350 × 450 mm^2) were used to package green asparagus spears (as described in "Materials" section) in the positive control group. Approximately 100 holes were punctured with needles on both sides of the bags to allow flow between the internal and external air. Moreover, treatment group 1 was treated with MAP (same formulation as in "Materials" section), whereas treatment group 2 (as a negative control) was directly injected into the acrylic cylinder without any addition. For treatment groups 1 and 2, an acrylic cylinder (220 mm length, 130 mm inner diameter, and 140 mm outer diameter) with the same internal volume as that of the glass cylinder was used (as shown in Sect. 2.6). The final VLDPE films were adhered to both sides of an acrylic cylinder using a quick-drying adhesive. The three groups of green asparagus spears were refrigerated at 5 °C to observe changes during the storage period (20 d). Each of the above groups contained 500 g of green asparagus spears (as described in "Materials" section), which were sampled once every four days for the analysis.

Quality indicators of green asparagus spear analysis

Fiber content analysis

The fiber content of green asparagus spears was analyzed following the method described by Bidwell and Walton [5]. A total of 8–10 green asparagus spears (approximately 100 g, W_0) were randomly sampled, cooked in boiling water for 15 min, washed with 200 mL of deionized water, and crushed in a homogenizer (2 min). The residue was filtered using a 30-mesh sieve and dried in an oven at 100 °C until a constant weight (W_1) was reached.

$$\text{Fiber content}(\%) = W_1/W_0 \times 100. \quad (9)$$

Vitamin C content analysis

The method for determining vitamin C (2, 6-dichlorophenolindophenol titrimetric method) was performed as described by Mottern et al. [22]. Green asparagus spears were crushed, and 20 g of asparagus juice was collected for determination. The samples were mixed with 20 mL metaphosphoric-acetic acid solution and homogenized for 1 min. The supernatant was transferred to a volumetric flask, diluted to 100 mL, and titrated with a phenol solution to calculate the vitamin C content.

Firmness measurement

This method was performed as described by Lin et al. [19] with minor modifications. In brief, for each group of 20 green asparagus spears, a texture analyzer (TA-XT plus C, Stable Microsystems, Godalming, UK) with a P5 plunger (5 mm) and a constant moving rate of 5 mm/min drop speed was used to determine the firmness at 10 cm below the tip of the square, and the mean values were expressed as force (N).

Chlorophyll content analysis

The method reported by Huang et al. [11] was applied, with minor modifications. A 100 g sample of green asparagus spears was weighed, added to 500 mL acetone and 2 g calcium carbonate, crushed by a homogenizer, and then filtered through 300 mL 80% acetone until colorless. Finally, 100 mL of the filtrate was quantified using 80% acetone. A spectrophotometer was used to determine the absorbance of the filtrate at 665 nm and 649 nm. The formula for calculating chlorophyll content is as follows.

$$\text{Chlorophyll content} = 6.45 \times A_{665} + 17.72 \times A_{649}. \quad (10)$$

The chlorophyll content was expressed in ppm of 80% acetone.

Alcohol-soluble saccharide content determination

The alcohol-soluble saccharide content of the samples was determined using the method described by Wu et al. [39] with some modifications. Five green asparagus spears were randomly collected, cut into slices, freeze-dried, and milled into a powder with a grinder. A dried powder sample (0.02 g) was extracted with 5 mL 80% alcohol in a water bath at 70 °C for 30 min. The mixture was centrifuged at 100×*g* for 10 min to remove the upper clarified solution. The precipitate was extracted twice, as described above. The supernatants of the three extracts were collected using a vacuum rotary evaporator to remove the alcohol and water. Finally, 1 mL of distilled water was added to dissolve the pasty substance in the bottles, and the resulting mixture was prepared for further use. A total of 0.02 mL of the above sample was obtained, diluted to 5 mL with deionized water, and mixed well with a vortex oscillator. Then, another 1 mL sample was collected and added to a 5% phenol solution (0.5 mL) and 2.5 mL sulfuric acid solution. The solution was then mixed and incubated in a water bath at 25 °C for 10 min. Finally, the absorbance was measured at 490 nm using a spectrophotometer. A standard curve was plotted using glucose (10–100 μg/mL). The alcohol-soluble saccharide contents of the samples were then calculated. Each unit consisted of the glucose (μg)/sample (dry weight) per gram.

Equation derivation

MATLAB® (Mathworks, Inc. Natick, MA, USA) software package was used to calculate balanced mass equations. O_2 and CO_2 mass balance equations were developed, and their contents at each time point were obtained.

Statistical analysis

All measurements were performed at least in triplicates. The values in the tables and figures represent means ± standard deviation (SD). Statistical analyses were performed using SAS software version 9.1 (SAS Institute Inc., Cary, NC, USA) for the analysis of variance. If the values were significantly different at a significance level of 0.05, Duncan's multiple range test was used to assess the statistical significance of the differences between means.

Results and discussion

Reaction rate and rate equation for simulating the consumed O_2 and produced CO_2

The reaction mechanism of the active MAP developed in this study involves the provision of water by the hygroscopic effect of calcium chloride, which facilitates a rapid atmospheric reaction. Sodium ascorbate and ferrous sulfate react and consume O_2. Sodium carbonate was reacted to produce CO_2.

Reaction and consumption of O_2:

$$\text{monoanion of ascorbic acid} + 1/2\ O_2 \rightarrow \text{dehydroascorbic acid} + OH^-, \quad (11)$$

$$Fe^{2+} + 1/4\ O_2 + 21/2H_2O \rightarrow Fe(OH)_3 + 2H^+. \quad (12)$$

Reaction of CO_2 production:

$$CO_3^{2-} + 2H^+ \rightarrow CO_2 + H_2O. \quad (13)$$

The autoxidation rate constants of sodium ascorbate and ferrous sulfate at 5 and 25 ℃ were analyzed and calculated from the rate constants of the reaction between carbonate and hydrogen ions, as reported by Shen et al. [33]. From the above equation of the reaction mechanism, the rate equations of the O_2 consumed and CO_2 produced by the regulator were established as follows:

$$\begin{aligned}&\text{Rate equation of } O_2\text{consumed}: -d[O_2]\\&= -0.25 \times K_2 \times \left[Fe^{2+}\right] \times [O_2]^{0.25}\\&\quad - 0.5 \times K_1 \times [SA] \times [O_2]^{0.5},\end{aligned} \tag{14}$$

$[O_2]$: Value of dissolved O_2 in the solution (mole/L); $[Fe^{2+}]$: Content of ferrous ions in the solution (mole/L); [SA]: Content of sodium ascorbate in the solution (mole/L); K_1: Autoxidation rate constant of ascorbic acid ($L^{3/2}\ mol^{-0.5}\ s^{-1}$); K_2: Autoxidation rate constant of ferrous ions ($L^{5/4}\ mol^{-0.25}\ s^{-1}$).

$$\begin{aligned}&\text{Rate equation of } CO_2\text{produced}: d[CO_2]/dt\\&= K_3 \times [SC] \times \left[H^+\right]^2,\end{aligned} \tag{15}$$

$[CO_2]$: Content of CO_2 in the solution (mole/L); [SC]: Content of sodium carbonate in the solution (mole/L); $[H^+]$: Content of hydrogen ions in the solution (mole/L); k_3: Reaction rate constant ($L^3\ mol^{-2}\ s^{-1}$).

In the CO_2 generation reaction, the H^+ ion is one of the primary reactants, and the source of H^+ ions is the oxidation process of Fe^{2+} ions, whose rate equation is as follows:

$$\begin{aligned}d\left[H^+\right]/dt =& 2 \times K_2 \times \left[Fe^{2+}\right]\\&\times [O_2] - 0.25 - 2 \times K_3 \times\\&[SC] \times \left[H^+\right]^2.\end{aligned} \tag{16}$$

To calculate the reaction rate, the saturation concentrations of the reactants were used in the equations mentioned earlier. The MAP design in this study provides water through the absorption of calcium chloride to dissolve reagents in a molten state [8]. Therefore, it was assumed that the dissolved MAP reagents would reach saturation solubility in the liquid phase.

Mass transfer systems and rate equations of O_2 and CO_2

In this study, the reagents in the MAP consumed the O_2 in the liquid phase, whereas O_2 in the gas phase continuously diffused into the liquid phase. Hence, using film theory to analyze the gas–liquid two-phase O_2 transport phenomenon, the gas–liquid mass transfer coefficients were divided into two main phases: the gas-phase (K_g) and liquid-phase (K_L) mass transfer coefficients [16, 44]. In general, the difference in the concentration and resistance of the gas phase compared with that of the liquid phase was significantly smaller. Thus, only the gas–liquid two-phase mass transfer coefficient was used to investigate the liquid phase. The O_2 diffusion rate equation for the gas phase in the liquid phase is as follows:

$$d[O_2]/dt = K_L \times \left([O_2]^* - [O_2]\right), \tag{17}$$

$[O_2]^*$: Saturation concentration of O_2 in the solution (molar); $[O_2]$: Concentration of O_2 in the solution (molar); K_L: Mass transfer coefficient of O_2 in the liquid phase (s^{-1}).

The reagents in the MAP reaction of the liquid phase produced CO_2 because the difference the concentration between the gas and liquid phases was caused by CO_2 mass transfer into the gas phase. The moisture content of the MAP formulation was low because the reagent reacted in a molten state. Therefore, the CO_2 saturation concentration in the liquid phase is reached. Thus, the mass transfer resistance was only observed from the liquid phase to the gas phase. The mass transfer rate of CO_2 from the liquid phase to the gas phase is expressed as follows:

$$d\left[C_g\right]/dt = K_g \times \left(C_g^* - C_g\right), \tag{18}$$

C^*_g: Saturation concentration of CO_2 in the gas phase (molar); C_g: Concentration of CO_2 in the gas phase (molar); K_g: Mass transfer coefficient of CO_2 in the gas phase (s^{-1}).

Vapor permeability of packaging film material and respiration rate of green asparagus spears

This study used a VLDPE film with a high O_2 permeability. According to a previous report, film packaging with high O_2 permeability is appropriate for asparagus [42]. During packaging by film, gas spreads owing to the difference in atmospheric concentration inside and outside the system. Therefore, MAP systems commonly use low O_2 and high CO_2 gas compositions to extend the shelf life of food. Hence, the atmospheric permeability of packaging films is an important factor that affects food quality during storage [16, 42]. In this study, the O_2 and CO_2 permeability coefficients of the VLDPE films were measured using instrumental analysis. Fick's 1st law calculated the O_2 and CO_2 diffusion rates in an MAP system [16]. According to a previous report, the respiration rate of asparagus at 5 °C is approximately 60 mg CO_2/Kg/h, which causes rapid maturation and induces senescence [23, 30]. Accordingly, green asparagus spears can retain a particular physiological influence of MAP at 5 °C. Therefore, O_2 and CO_2 composition changes in green asparagus spears caused by respiration in the cylinder at 5 °C for 120 h were analyzed. The gas content was established

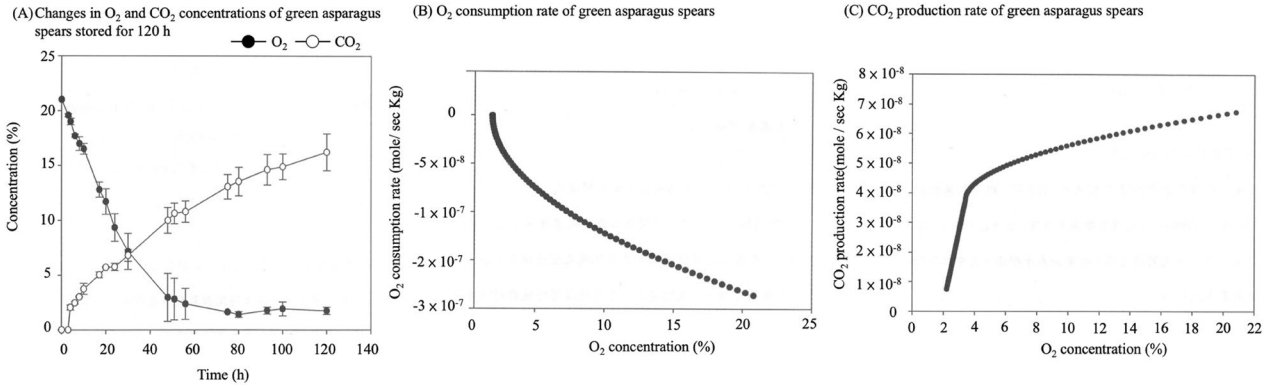

Fig. 2 Atmospheric changes, O_2 consumption rate, and CO_2 production rate of green asparagus spears stored in a closed system at 5 °C for 120 h (storage of 800 g green asparagus spears in a 2920 mL breathing cylinder). **A** Changes in O_2 and CO_2 concentrations of green asparagus spears stored for 120 h. **B** O_2 consumption rate of green asparagus spears. **C** CO_2 production rate of green asparagus spears

and the relationship between the time equations was determined. Following the differentiation of the above equations over time, the O_2 reduction and CO_2 production rates under different gas compositions were determined. The values obtained can be used to estimate the O_2 and CO_2 respiration rates in green asparagus spears under different gas compositions.

Temperature and atmospheric composition affected the respiration rate of green asparagus spears. Therefore, for storage, MAP packaging with low temperature, low O_2, and high CO_2 significantly reduces the respiration rate of green asparagus spears. The use of high O_2 in MAP (60% and 80%) led to increased respiration of asparagus, which caused the excessive accumulation of CO_2 and O_2 depletion in the package. In addition, lignin deposition and progression are effectively retarded, but the texture of asparagus becomes tender [26]. In the MAP system, respiration of green asparagus spears also affected the atmospheric composition of packaging system. First, a relationship between O_2 consumption and CO_2 generation was observed in a closed system of green asparagus spears at 5 °C for 120 h. The results showed that when the storage period reached 120 h, respiration of green asparagus spears consumed 1.97% O_2 and produced 17.4% CO_2 (Fig. 2A). The O_2 levels were balanced after 75 h. Meanwhile, the CO_2 level was generated more rapidly in the early storage stage, but slowed down in the later stage. The O_2 and CO_2 concentration equations were regressed numerically and are expressed as follows:

$$\text{Equation for } O_2 \text{ concentration: } C_{O_2} = 2 \times 10^{-12}t^2 - 0.000001t + 0.204, \quad (19)$$

$R^2 = 0.9813$,

C_{O2}: O_2 concentration (%); t: Time (s).

$$\text{Equation for } CO_2 \text{ concentration: } C_{CO_2} = 6 \times 10^{-13}t^2 + 6 \times 10^{-7}t + 0.0098, \quad (20)$$

$R^2 = 0.9747$, C_{CO2}: CO_2 concentration (%); t: Time (s).

The above results (Fig. 2A) were differentiated by time to visualize the rate of O_2 consumption per unit of time. In green asparagus spear packaging systems, O_2 consumption is caused by respiration. Thus, the rate of O_2 consumption by green asparagus spears is expressed as follows:

$$\text{Consumption rate of } O_2 = -\mathrm{d}[O_2]/\mathrm{d}t = 4 \times 10^{-13}t - 1 \times 10^{-7}, \quad (21)$$

$[O_2]$: Mole of O_2 in green asparagus spear packaging system (moles); t: Time (s).

As mentioned above, combining the O_2 concentration relationship and consumption rate equation can be used to obtain the O_2 consumption rate of green asparagus spears under different O_2 concentrations (Fig. 2B). The relationship between O_2 concentration and consumption rate is as follows:

$$yO_2 = 4 \times 10^{-10}x^2 - 2 \times 10^{-8}x + 1 \times 10^{-8}, \quad (22)$$

$R_2 = 0.9837$, yO_2: $\mathrm{d}[O_2]/\mathrm{dt}$ (unit: mol/s).

However, the generation of CO_2 in the packaging system is caused by the respiration of green asparagus spears, and the CO_2 production rate equation is expressed as follows:

$$\mathrm{d}[CO_2]/\mathrm{d}t = -1.2 \times 10^{-13}t + 5 \times 10^{-8}, \quad (23)$$

$\mathrm{d}[CO_2]/\mathrm{d}t$: CO_2 production rate (mole/s); t: Storage time (s).

Combined with the CO_2 concentration relationship and production rate equation, the CO_2 production rate of green asparagus spears at different O_2 concentrations was obtained (Fig. 2C).

The relationship between O_2 concentration and CO_2 production rate is as follows:

$$yCO_2 = 2 \times 10^{-8} \ln x + 3 \times 10^{-9}, \quad (24)$$

$R^2 = 0.9282$, $yCO_2 = d\ [CO_2]/dt$ (unit: mole/s); x: O_2 concentration (%).

This study used the gas permeability of the LDPE film as a packaging film, and the results revealed that the permeability (cc-mil/m^2-24 h) of CO_2 (10,415 ± 438) was about fourfold that of O_2 (2395 ± 147) at 5 °C.

The atmosphere of the MAP system was used to determine compositional changes in the equation mode of verification. MAP formulation reagents were dissolved in the liquid phase for oxidation and CO_2 production. O_2 molecules from the gas phase were mass-transferred to the liquid phase to react with the agent. However, the opposite is true for CO_2. The relationship between the mass transfer rate of O_2 and the rate of chemical reaction is expressed as follows:

$$\text{When the mass transfer stabilized, } F_1 = F_2, \quad (25)$$

F_1: O_2 mass transfer rate; F_2: Oxidation rate of the MAP formulation reagents.

$$F_1 = K_L(C_0 - C_1), \quad (26)$$

K: mass transfer coefficient; C_0: equilibrium concentration of O_2 at the liquid-phase interface; C_1: bulk concentration of O_2 in the liquid phase.

$$F_2 : \text{ Oxidation rate of the MAP formulation reagents} = -0.25 \times K_2 \times \left[Fe^{2+}\right] \times [O_2]^{0.25} - 0.5 \times K_1 \times [SA] \times [O_2]^{0.5}. \quad (27)$$

As the oxidation rate of the MAP formulation reagents outweighed the mass transfer rate of O_2, the oxidation rate of MAP formulation reagents was controlled by the mass transfer rate of O_2. The O_2 mass transfer rate equation was $F_1 = K\ (C_0 - C_1)$. In this study, the mass transfer rate constant (K) was obtained from the liquid-phase mass transfer image (K_L: 1.4515×10^{-5} (1/s)) and the rapid oxidation reaction of the MAP formulation reagents in the liquid phase. Thus, C_1 is assumed to be zero. Henry's law estimated C_0:

$$\text{Henry}'\text{slaw} P_A = H \times X_A, \quad (28)$$

P_A: partial pressure of O_2 (atm); H: Henry's constant (atm/mole frac.); X_A: mole fraction of A in liquid.

The internal difference method was used to obtain Henry's constant, and the O_2 at 5 °C was 29,100 (atm/mole fraction). Therefore, through calculations under different O_2 pressures, the solubility of O_2 in the liquid phase was obtained as C_0. In the observation of MAP in the pretest at 5 °C after a 24 h reaction, the O_2 concentration stabilized, and the atmosphere with the MAP system changed in two periods. The first stage (first 24 h) involved the MAP deoxygenation rate simulation. The second stage (after 24 h) included the gas concentration for the packaging film permeability controlled by the gas rate. The equation models calculated using theoretical and experimental values were compared (Fig. 3A). The observed and theoretical values for the first stage exhibited matching trends, confirming the accuracy of using the O_2 mass transfer rate to predict the MAP deoxygenation rate. In the second stage, the O_2 concentration increased with time owing to the gas permeability of the packaging film, which caused the O_2 outside to diffuse into the package with a difference in concentration.

Nevertheless, the experimental value was higher than the theoretical value, probably because of the increased practical permeability of the VLDPE film during packaging and storage. The measurements were performed at 5 °C and 0% relative humidity. However, in the practical packaging experiment, the relative humidity of the 5 °C storage environment may have affected the permeability of the VLDPE film. The equation for the CO_2 production rate of the MAP is expressed as follows:

$$d[CO_2]/dt = K_g \times \left(C_g^* - C\right), \quad (29)$$

K_g: CO_2 mass transfer rate constant (1/s); C^*_g: equilibrium concentration of CO_2 at the gas-phase interface; C: CO_2 concentration in the gas phase.

Henry's law estimated the equilibrium concentration of CO_2 at the gas-phase interface, and the equation is as follows:

$$P_A = H \times X_A, \quad (30)$$

P_A: Partial pressure of carbon dioxide (atm); H: Henry's constant (atm); X_A: mole fraction of A in liquid.

As for Henry's constant, when $t = 0$,

$$C_g^* = H \times X_{A0}, \quad (31)$$

where X_{A0} is the mole fraction of the CO_2 saturation concentration (solubility) in water at 5 °C.

The saturation concentrations of CO_2 at 0 and 10 °C were 0.3346 and 0.2318 g/100 g H_2O, respectively, and the saturation concentration at 5 °C was estimated to be 0.2832 g/100 g H_2O [35]. The theoretical and

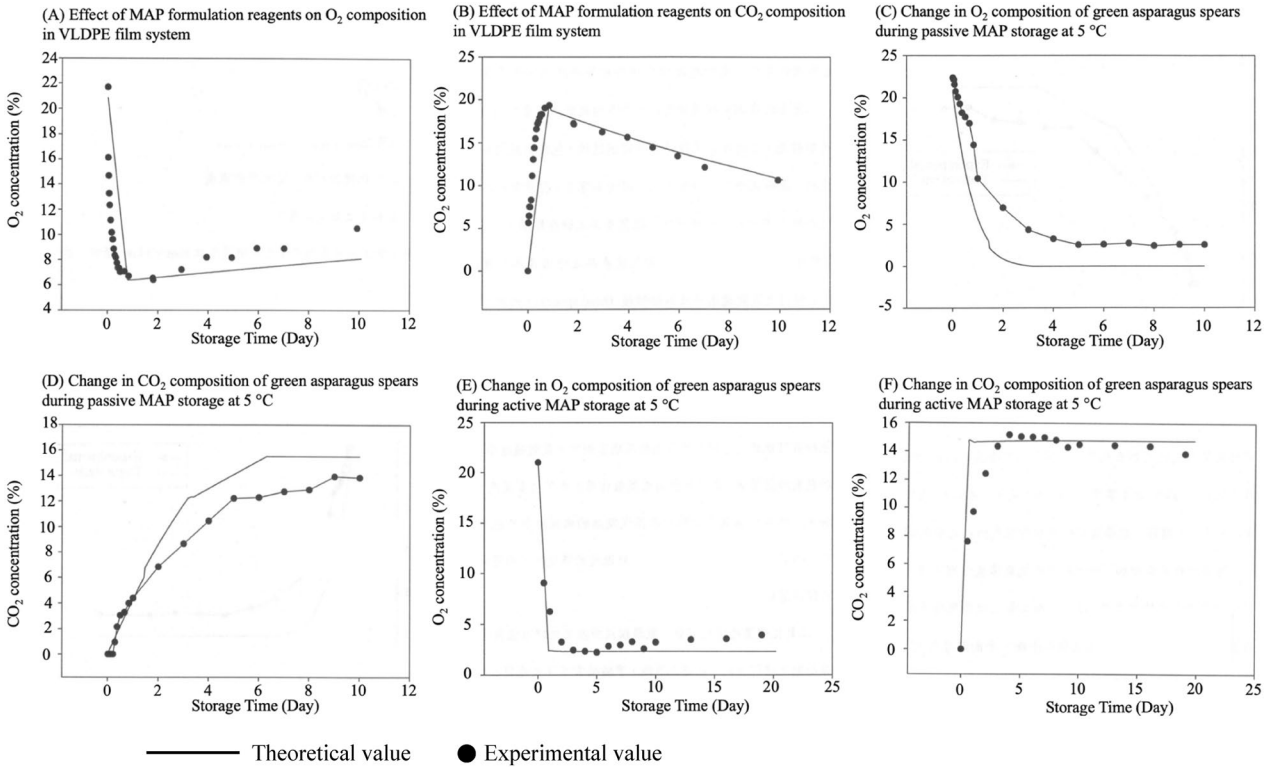

Fig. 3 Equations (theoretical value) and practical validation (experimental value) of each factor in the MAP system, including the atmospheric composition. **A** Effect of MAP formulation reagents on O_2 composition in the VLDPE film system. **B** Effect of MAP formulation reagents on CO_2 composition in the VLDPE film system. **C** Changes in O_2 composition of green asparagus spears during passive MAP storage at 5 °C. **D** Changes in CO_2 composition of green asparagus spears during passive MAP storage at 5 °C. **E** Changes in O_2 composition of green asparagus spears during active MAP storage at 5 °C. **F** Changes in CO_2 composition of green asparagus spears during active MAP storage at 5 °C

experimental values obtained using the equation model were compared (Fig. 3B). The experimental and theoretical values in the first stage were similar, confirming the correctness of the CO_2 production rate equation of the MAP formulation in terms of CO_2 mass transfer rate. In the second stage, the theoretical and experimental values exhibited a similar trend, confirming the accuracy of the observed CO_2 permeability of the VLDPE film at 5 °C.

Synthesis of MAP system for green asparagus spears

The chemical reaction rate equation of the MAP formula was used to establish the respiration rate of green asparagus spears, O_2 permeability of the packaging film, and the O_2/CO_2 mass transfer rate equation. The above equations can be applied to the MAP system of green asparagus spear O_2 and CO_2 during the storage period. When the atmospheric concentration changes, the O_2 and CO_2 balance equations become as follows:

O_2 mass balance relationship:

$$-\mathrm{d}[O_2]/\mathrm{d}t = -R^{T}_{\text{agent }O_2} - WR^{T}_{O_2} + P_O A/X\left(O_2^{ext} - O_2^{pkg}\right), \tag{32}$$

$R^{T}_{\text{agent }}O_2$: The O_2 consumption rate of MAP formulation reaction (mL O_2 / sec); W: Weight of green asparagus spears (kg); R^{T}_{O2}: Respiration rate of green asparagus spears (mL O_2/s); P_{O2}: O_2 permeability of VLDE film (mL mil/m^2 s); *A*: Area of packaging film (m^2); *X*: Thickness of packaging film (mils, 1 mil = 1/1000 in or 25.4 μm); O_2^{ext}: O_2 concentration in the environment (%); O_2^{pkg}: O_2 concentration in the packaging system (%).

CO_2 mass balance relationship:

$$\mathrm{d}[CO_2]/\mathrm{d}t = -R^{T}_{\text{agent }CO_2} - WR^{T}_{CO_2} + P_{CO_2}A/X\left(CO_2^{ext} - CO_2^{pkg}\right), \tag{33}$$

$R^{T}_{\text{agent }CO2}$: CO_2 consumption rate of MAP formulation reaction (mL CO_2/s); W: Weight of green asparagus spears (kg); R^{T}_{CO2}: Respiration rate of green asparagus spears (mL CO_2/s); P_{CO2}: CO_2 permeability of VLDE film (mL mil/m^2 s); *A*: Area of packaging film (m^2); *X*:

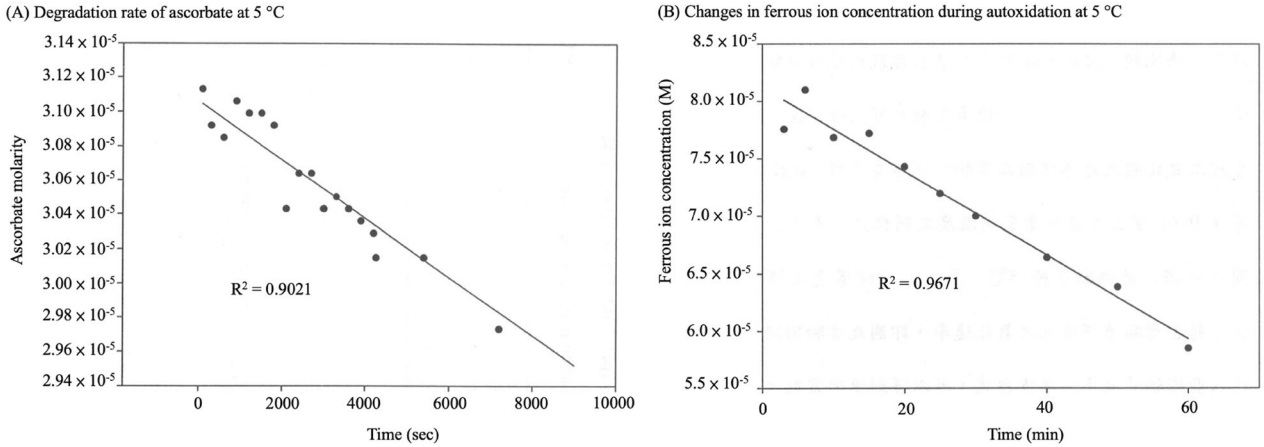

Fig. 4 Reaction rate constants of the reagents for active MAP formulations. **A** Degradation rate of ascorbate at 5 °C. **B** Changes in ferrous ion concentration during autoxidation at 5 °C

Thickness of packaging film (mils, 1 mil = 1/1000 in or 25.4 μm); CO_2^{ext}: CO_2 concentration in the environment (%); CO_2^{pkg}: CO_2 concentration in the packaging system (%).

However, the chemical reaction rate of the reagents in MAP is relatively high. Thus, the rate of mass transfer of O_2 from the gas to the liquid phase and that of CO_2 from the liquid phase to the gas phase may be the key factors controlling the overall MAP reaction rate. As the mass transfer rate was assumed to be the rate-determining step of the reaction, the mass balance equation is expressed as follows:

The O_2 mass balance equation is:

$$-\mathrm{d}[O_2]/\mathrm{d}t = -F_{O_2} - WR^{T}_{O_2} + P_{O_2}A/X\left(O_2^{ext} - O_2^{pkg}\right), \quad (34)$$

F_{O2}: O_2 mass transfer rate (mole/s).

The CO_2 mass balance equation is

$$\mathrm{d}[CO_2]/\mathrm{d}t = F_{CO_2} + WR^{T}_{CO_2} + P_{CO_2}A/X\left(CO_2^{ext} - CO_2^{pkg}\right), \quad (35)$$

F_{CO2}: CO_2 mass transfer rate (mole/s).

Reaction rate constants of O_2 consumed and CO_2 produced by the MAP formulation reagents

The MAP formulations used in this study consisted of sodium ascorbate, ferrous sulfate, sodium carbonate, and calcium chloride. In the initial stage of the reaction, calcium chloride absorbed moisture to provide water, and the reagents were dissociated in the solution. The negative ions consisted of ascorbic acid, sulfate, carbonate, argon carbonate, and chloride, and the positive ions were sodium, ferrous, and calcium. As the reagents in MAP dissociated to form a complex solution, to simplify and facilitate the establishment of the MAP reaction mechanism and rate equation, we established the reaction mechanism and measured the reaction rate constants for the reactants that directly consumed O_2 and produced CO_2. The reagents in the MAP formulation were sodium ascorbate and ferrous sulfate, which consumed O_2, and sodium carbonate, which produced CO_2. Therefore, the reaction rate constants at 25 °C and 5 °C were analyzed for the autoxidation of ascorbic acid, which dissociated from sodium ascorbate, the autoxidation of Fe^{2+} ions, which dissociated from ferrous sulfate, and the CO_3^{2-} reaction from sodium carbonate.

Figure 4A shows the degradation rate of ascorbic acid at 5 °C. The value was regressed to obtain a straight line, and the slope of this line is the degradation rate of ascorbic acid. The rate of degradation of ascorbic acid at 5 °C was obtained by substituting the rates of degradation, which were 1×10^{-10} and 2×10^{-9} s^{-1} at 25 °C, into the oxidation rate equation. This rate constant represents the temperature dependence. The reaction was slow at low temperatures (5 °C) and the rate constants were minor; however, at 25 °C, the opposite was true. The difference between the above two results was 20 folds, whereas the findings obtained at 25 °C were similar to those of previously published studies. However, the available literature lacks information to compare the results at 5 °C. The validity of this method was verified using the rate constants at 25 °C. Accordingly, the reliability of the 5 °C rate constant is indirectly confirmed.

The rate constant of the carbonic acid reaction with CO_2 is difficult to obtain [21]. Therefore, the relationship between the regular rate and the temperature established

by Pines et al. [25] was used. Figure 4B shows the relationship between the change in the concentration of Fe^{2+} ions and the time during the autoxidation reaction at 5 ℃. The experimentally established oxidation rate (slope after regression) can be substituted into the ferrous ion oxidation rate equation to obtain the autoxidation rate constants for ferrous ions, namely, 0.02737 and 0.0014117, at 25 °C and 5 °C, respectively. Thus, ferric ions (Fe^{3+}) are good reductants for promoting the oxidation rate of Fe^{2+} [10].

Mass transfer rates of O_2 and CO_2

The mass transfer rate of O_2 is an important determining step in the MAP formulation reaction to consume O_2. Therefore, the mass transfer rate of O_2 significantly affected the deoxygenation rate of the MAP formulation. At low temperatures, the saturation solubility of O_2 in solution and O_2 mass transfer coefficient increased. In contrast, the opposite trend was observed at high temperatures. In this study, the solution's oxygen mass transfer coefficient (KL) at 5 °C was 1.4515×10^{-5} (1/s). The CO_3^{2-} in the MAP formulation reacted with H^+ ions to form CO_2, which was released from the liquid phase to the gas phase via a mass transfer mechanism. Therefore, the mass transfer rate of the gas phase may be a determining factor for the rate of CO_2 production in the gas phase. In this study, the mass transfer coefficient (K_g) of CO_2 in the solution at 5 °C was 2.91667×10^{-6} (1/s).

Comparison of rates of chemical reactions and mass transfer

This study analyzed several parameters, including the reaction rate constants, gas mass transfer coefficients (O_2 and CO_2), and solubilities (g/100 mL) of sodium ascorbate, ferrous sulfate, and sodium carbonate (61.98, 24.49, and 35.19, respectively). The chemical reaction rate of MAP is faster than the mass transfer rates of oxygen and carbon dioxide. Therefore, the mass transfer rate was the main factor controlling the O_2 consumption and CO_2 production.

Relationship between MAP formulation and volume

The MAP used in this study was placed in a closed volume of 285 mL headspace at 5 °C and the formulations were reacted for 48 h. The O_2 content was reduced to 65% and the CO_2 content increased to 15.5%. Therefore, according to the ideal gas equation, each MAP consumed 1.8117×10^{-3} mol O_2 and produced 1.9366×10^{-3} mol CO_2. Hence, to apply MAP to different headspaces, the formula dosage was multiplied by the volume ratio, expressed as the volume divided by 285 mL.

Passive and active MAP systems

The factors that affect MAP include the respiration rate of the packaging product, product weight, permeability of the packaging film, and the headspace. The package permeability was sufficient to maintain the required gas concentration inside the MAP system, thus enabling the maintenance of the O_2 and CO_2 concentrations during storage [17]. A passive MAP system must consider the relationship between these four factors. Green asparagus spears (500 g) were wrapped in VLDPE film. The film area was 0.0265 m^2 and the headspace was 2073 mL. The experimental and theoretical values of the O_2 and CO_2 concentration changes in the packaging system were determined at 5 °C for 10 days (Fig. 3C, D). The theoretical value was calculated by combining the relationship between the respiration rate of green asparagus spears, the gas concentration, and the permeability of the VLDPE film.

$$d[O_2]/dt = -wR_{O_2}^{T} + P_{O_2}A/X\left(O_2^{ext} - O_2^{pkg}\right), \tag{36}$$

$$d[CO_2]/dt = -wR_{CO_2}^{T} + P_{CO_2}A/X\left(CO_2^{ext} - CO_2^{pkg}\right). \tag{37}$$

A theoretical equation was used to calculate whether the O_2 and CO_2 concentration trends during the storage period matched the measured values. However, compared with the measured values, the decrease in the rate of O_2 concentration was higher, and the increase in the rate of CO_2 concentration was slightly higher after 2 days. Possible reasons for these differences are as follows. First, the actual respiration rate of green asparagus spears in the packaging system was lower than predicted. Secondly, the practical permeability of the VLDPE film during storage was higher than the measured value. As the respiration rate equation established in the closed system showed high permeability compared with the semipermeable system in practical applications, the respiration rate of green asparagus spears in the practical packaging system may be slightly lower than the estimated value obtained from the rate equation established for the closed system. In addition, the evaporation of green asparagus spears produces many vapors. Water vapor condensation droplets were observed in the packaging system during storage trials and were attached to the inner wall of the packaging system. Therefore, higher permeability can be obtained in a 100% relative humidity environment. As mentioned above, changes in O_2 and CO_2 concentrations in the passive MAP system were estimated using the equation model established in this study. However, the film permeability should be measured at 100% relative humidity to enhance prediction accuracy.

Moreover, the active MAP system used in this study had to control the O_2 and CO_2 concentrations of packaging by chemical reactions of reagents to achieve the desired atmospheric composition. The O_2 and CO_2 mass transfer rate equations established above, green asparagus spears at a 5 ℃ respiration rate, and gas composition of the relationship equation with the packaging film permeability were established in the active MAP system of O_2 and CO_2 with a mass balance equation, with the formulas presented as follows:

$$d\,[O_2]/dt = -F_{O_2} - WR^{T}_{O_2} + P_{O_2}A/X\left(O_2^{ext} - O_2^{pkg}\right), \quad (38)$$

$$d\,[CO_2]/dt = -F_{CO_2} + WR^{T}_{CO_2} - P_{CO}A/X\left(CO_2^{ext} - CO_2^{pkg}\right), \quad (39)$$

$F_{O2}=O_2$ mass transfer rate (mole/s); $F_{CO2}=CO_2$ mass transfer rate (mole/s).

The above equations were used to estimate the theoretical O_2 and CO_2 concentrations for the active MAP system used in this study at 5 °C storage, and the results were compared with the measured data obtained from the practical packages (Fig. 3E, F). For variations in O_2 concentrations, the theoretical values were consistent with the measured values for up to five storage days, confirming the applicability of the equation model to describe active MAP. An evident upward trend was observed in the measured O_2 values on day 5, but no significant change was detected in the theoretical O_2 concentrations on days 5–20. This discrepancy was related to the senescence of green asparagus spears and errors in determining membrane permeability. As the storage time increased, the respiration rate of green asparagus spears decreased with senescence. The respiration rate of green asparagus spears in the equation model was expressed when the physiological effect was average, resulting in a difference. On the other hand, the VLDPE packaging film most likely caused the vapor dispersion of green asparagus spears, which was the same as the case of passive MAP at 100% relative humidity, possibly leading to higher gas permeability. As for CO_2 changes, the theoretical and practical values estimated by the equation model showed the same trend at the initial stages of accumulation. Later, the tendency of the observed values decreased, and the theoretical values remained balanced. The influence of the theoretical difference is consistent with the above results.

Changes in the atmospheric composition of passive and active MAP systems in the preservation of green asparagus spears

Thus far, a suitable atmosphere for asparagus (7% CO_2 and 15% O_2) can provide a shelf life of 14 d at 5 °C (necessary to inhibit microorganisms) [16, 42]. The changes in the atmospheric composition of the package during the storage period of the passive MAP system (Fig. 5A) revealed that the O_2 concentration gradually decreased with increasing storage time. On day 6 of

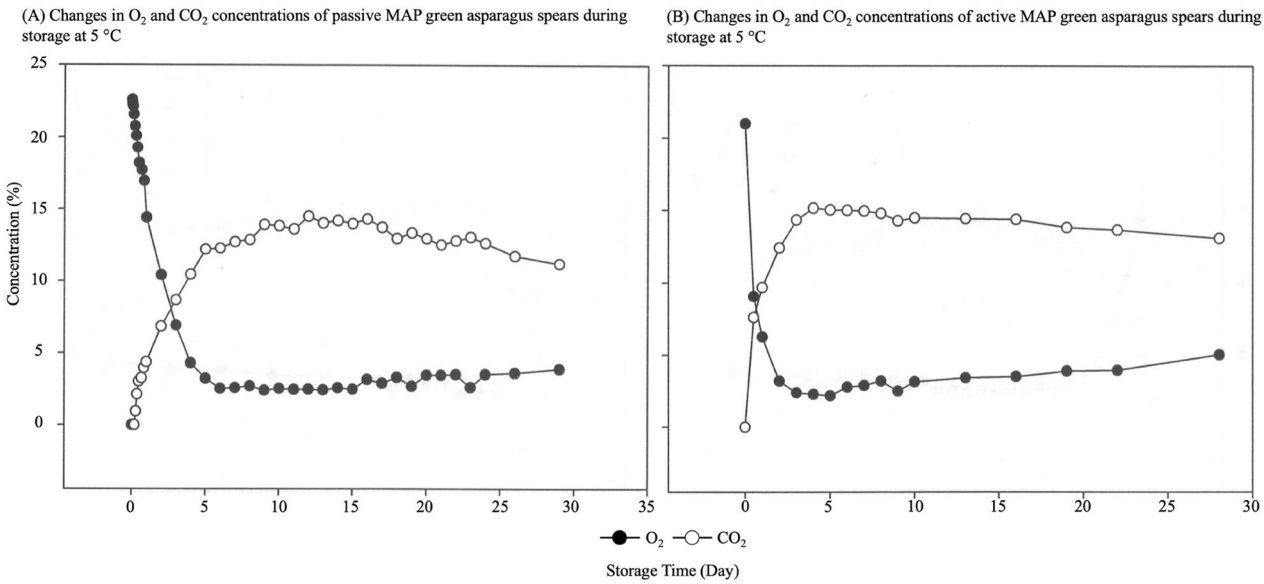

Fig. 5 Effects of passive and active MAP on atmospheric composition changes in the breathing cylinder of green asparagus spears during storage at 5 °C. **A** Changes in O_2 and CO_2 concentrations of passive MAP green asparagus spears during storage at 5 °C. **B** Changes in O_2 and CO_2 concentrations of active MAP green asparagus spears during storage at 5 °C

achieving balance, the average O_2 concentration was 1.5%. Meanwhile, the CO_2 concentration increased with storage time and reached equilibrium on storage day 8 at a concentration of 15%. In contrast, the active MAP equation estimated that O_2 and CO_2 concentrations in the package would reach 6.6% and 14.25%, respectively, on day 2. As shown in Fig. 5B, the O_2 concentration reached equilibrium (3.2%) after 2 days of storage. In addition, the CO_2 concentration reached equilibrium (15%) 3 days after storage. The asparagus MAP, O_2, and CO_2 generally reach equilibrium on days 15 and 13, with a total shelf life of 23 days [42]. Notably, the O_2 concentration was 3% lower than intended and that of CO_2 was close to the theoretical value. Thus, the active MAP formulations effectively reduced O_2 in the package while producing CO_2 compared with the control group, in which the active MAP can quickly balance the atmosphere in the package.

Effects of passive and active MAP on qualities of green asparagus spears during preservation

Fiber content

The fiber content of the green asparagus stem is a significant factor that influences quality and edibility [37]. However, green asparagus spears suffer from enzymatic effects, such as those of phenylalanine ammonia-lyase (PAL), cinnamyl alcohol dehydrogenase (CAD), peroxidase (POD), peroxidation, and isomeric peroxidation enzymes during storage, increasing lignin content [6, 20, 26, 36]. The fiber content of the control group (exposed to air) increased, whereas that of treatment group 1 (active MAP) decreased slightly with storage time (Table 1). A significant difference was observed in the fiber content of treatment groups 1 and 2 (sealed packing) after eight storage days ($p < 0.05$). In other words, using the MAP system can retard the increase green asparagus spear fiber content. As a result of the chemical reaction of the reagents in the MAP formulations, O_2 was consumed, CO_2 was released, and the atmosphere in the package was balanced after 2 days. In contrast, treatment group 2 consumed O_2 via the respiration of green asparagus spears, and equilibrium concentration was reached on day 6, leading to increased fiber production. Hence, the texture of asparagus spears must be preserved for as long as possible to extend their shelf life. Tian et al. [36] observed that using a prepared coating extended the shelf life of green asparagus spears from 5 to 7 days and reduced its permeability for water vapor, O_2, and CO_2, in addition to the production of lignin. Treatment with sucrose, which is mainly applied to the synthesis of cell wall components rather than to respiration and therefore inhibits senescence symptoms, results in a mechanism that maintains the firmness of asparagus spears by retarding the decomposition of protopectin and inhibiting the increase in water-soluble pectin content [23]. In parallel, maintaining the level of lignin in fresh products, which remains unachievable with any applied treatment, is difficult. Lignin levels can be delayed or reduced [20].

Vitamin C content

Vitamin C is one of the most sensitive materials in fresh produce exposed to unfavorable handling and storage conditions [18, 37]. Its degradation in green asparagus spears decreases rapidly after harvesting, especially at high temperatures, and the storage of asparagus at low O_2 concentrations reduces its degradation [42]. Low O_2 concentration inhibits the activity of vitamin C oxidase, thus reducing the loss of vitamin C. According to the results (Table 1), the vitamin C content of the control group decreased with storage time, with a 42% loss after 20 days of storage. The vitamin C content in the treatment group showed no significant differences during the storage period. However, a significant difference was observed in the vitamin C content between treatment groups 1 and 2 after 8 days of storage ($p < 0.05$). In the case of active MAP, the O_2 in the package was consumed to retard the degradation of vitamin C in green asparagus spears. Therefore, the respiration of green asparagus spears could not reduce the O_2 concentration immediately until six days to reach the equilibrium concentration. Li and Zhang [18] treated asparagus with MAP (with a silicon gum film window) and showed a significant difference in the ascorbic acid content after 15 days of treatment, with a 40% loss after 30 days. Melatonin-treated asparagus had 31.21%–37.73% higher vitamin C content than the control group after 25 days of storage [6]. Enzyme activity cannot be inhibited rapidly, and the continuous biological effect causes further vitamin C degradation. As an agricultural product is a living and breathing product, it maintains active metabolism after harvesting [3].

Firmness change

Texture is a critical quality indicator of asparagus spears [23]. The study showed that the firmness of the control group increased significantly with storage period (Table 1). In contrast, the firmness of treatment group 1 showed no significant change after 20 days compared with the same number of storage days, and the firmness after 12 days of storage was significantly lower than that of treatment group 2 ($p < 0.05$), a trend consistent with the change in fiber content. The results showed that the application of active MAP significantly reduced O_2 and increased CO_2 concentrations within 2 days, inhibited fiber production during storage, and maintained the

Table 1 Changes in quality indicators of green asparagus spears during storage

Storage time (days)	Fiber content (%)			Vitamin C content (mg/100 g)			Firmness (*N*)			Chlorophyll content (ppm)			Alcohol-soluble saccharide content (μg/g)		
	Control	T1	T2	Control	T1	T2	Control	T1	T2	Control	T1	T2	Control	T1	T2
0	1.11 ± 0.15^{Ad}	1.11 ± 0.015^{Aa}	1.11 ± 0.15^{Aa}	24.51 ± 0.28^{Aa}	24.51 ± 0.28^{Ab}	24.51 ± 0.28^{Aa}	2057 ± 133^{Ac}	2057 ± 133^{Abc}	2057 ± 133^{Aab}	3.72 ± 0.12^{Aa}	3.72 ± 0.12^{Aa}	3.72 ± 0.12^{Aa}	0.28 ± 0.01^{Aa}	0.28 ± 0.01^{Aa}	0.28 ± 0.01^{Aa}
4	1.37 ± 0.07^{Ac}	0.49 ± 0.01^{Bb}	0.57 ± 0.03^{Bd}	18.65 ± 0.38^{Ab}	22.7 ± 0.00^{Ab}	19.90 ± 1.96^{Ab}	2294 ± 208^{Aa}	2244 ± 205^{Aa}	2181 ± 149^{Aa}	4.38 ± 0.24^{Aa}	4.09 ± 0.08^{Aa}	4.09 ± 1.29^{Aa}	0.21 ± 0.04^{Aa}	0.27 ± 0.10^{Aa}	0.26 ± 0.03^{Aa}
8	1.46 ± 0.03^{Ac}	0.48 ± 0.02^{Cb}	1.15 ± 0.06^{Ba}	18.49 ± 1.12^{Bb}	23.66 ± 0.21^{Ab}	17.64 ± 1.05^{Bd}	2165 ± 178^{Ab}	2129 ± 227^{Ab}	$2139 \pm 142A^{ab}$	3.38 ± 0.45^{Aa}	3.55 ± 0.40^{Aab}	3.15 ± 0.02^{Aa}	0.29 ± 0.05^{Aa}	0.24 ± 0.06^{Aa}	0.26 ± 0.02^{Aa}
12	1.74 ± 0.02^{Ab}	0.43 ± 0.04^{Cb}	0.76 ± 0.07^{Bb}	15.23 ± 0.12^{Cc}	24.86 ± 0.65^{Ab}	18.63 ± 0.43^{Bc}	2393 ± 117^{Aa}	2014 ± 148^{Cbc}	2194 ± 158^{Ba}	3.30 ± 0.82^{Aa}	3.20 ± 0.10^{Ab}	3.07 ± 0.19^{Aa}	0.27 ± 0.06^{Aa}	0.24 ± 0.05^{Aa}	0.26 ± 0.06^{Aa}
16	1.93 ± 0.03^{Aa}	0.48 ± 0.06^{Cb}	0.68 ± 0.08^{Bb}	12.80 ± 0.28^{Bd}	25.32 ± 0.64^{Ab}	23.87 ± 1.46^{Aa}	2412 ± 124^{Aa}	1965 ± 116^{Cc}	2167 ± 193^{Ba}	3.49 ± 0.54^{Aa}	3.45 ± 0.31^{Ab}	3.64 ± 0.33^{Aa}	0.21 ± 0.01^{Aa}	0.23 ± 0.06^{Aa}	0.22 ± 0.05^{Aa}
20	1.90 ± 0.02^{Aa}	0.37 ± 0.03^{Cb}	0.52 ± 0.04^{Bd}	10.38 ± 0.13^{Ce}	27.28 ± 0.13^{Aa}	20.38 ± 0.27^{Bb}	2347 ± 116^{Aa}	2014 ± 113^{Cbc}	2160 ± 167^{Ba}	3.44 ± 0.59^{Aa}	3.98 ± 0.36^{Aa}	3.36 ± 0.47^{Aa}	0.22 ± 0.05^{Aa}	0.22 ± 0.05^{Aa}	0.23 ± 0.04^{Aa}

Mean ± SD of values from triple trials

Means in the same column with different letters differ significantly ($p < 0.05$) according to Duncan's multiple range test

Means in the same row with different capitals differ significantly ($p < 0.05$) according to Duncan's multiple range test

T1: Treatment group 1, with active MAP

T2: Treatment group 2, with passive MAP (sealed packing)

Control: Control group, with no treatment, exposed to air

quality of green asparagus spears within a 20-day storage period. Moreover, it directly decreased the senescence of green asparagus with a significant reduction in oxidative enzyme activity.

One study indicated that although the firmness of each asparagus sample decreased over time, treatment with 3% sucrose extended its shelf life by 6 days [23]. Notably, MAP has been identified as an effective way to maintain improved color and appearance and higher levels of chlorophyll and vitamin C [42]. The electrostatic atomized water particle treatment for 90 min preserved the asparagus at 4 °C for 24 days, reduced the respiration rate and ethylene production, and inhibited enzymatic activities (PAL, CAD, and POD) associated with lignin and cellulose accumulation. In addition, treated asparagus retained its firmness after storage [20].

Chlorophyll content

Chlorophyll affects the color of green fruits and vegetables, and the chlorophyll enzymes of asparagus change to pheophytin during storage, causing the bright green surface of asparagus to change to a depressed dark green color. The storage of green vegetables in MAP reduces chlorophyll loss [1]. As shown in Table 1, no significant changes in chlorophyll were observed in either the control group or treatment groups 1 and 2 during the 20-day storage period. No significant differences were detected among the three groups on the same storage days. The storage period set in this study might be extremely short for observing chlorophyll in green asparagus spears using different packaging methods. Furthermore, the green asparagus spear samples used in this study were precooled to 5 °C, and the precooling step improved the preservation of chlorophyll. No significant changes were observed after 20 days. Li and Zhang [18] treated asparagus by MAP (with a silicon gum film window) and stored it by refrigeration (2 °C ± 1 °C) for 30 days at 95%–100% relative humidity in the package; the results showed a chlorophyll loss of 23%. Notably, one study revealed that total chlorophyll content decreased sharply from day 4 to the end of 24 days of storage [20]. Boonsiriwit et al. [6] also reported that the chlorophyll content in green asparagus decreased progressively with storage days (at 4 °C, relative humidity below 90%) and decreased by 20.93%–40.41% after 25 days of storage with melatonin treatment. A previous report mentioned that the controlled atmospheric storage of asparagus spears maintained a dark green color. In contrast, asparagus spears in general storage showed significant yellowing, with significant color differences between both, especially after the shelf life [1].

Alcohol-soluble saccharide content

Photosynthesis provides sugars for plant growth. In addition, respiration consumes sugars to produce ATP during harvest; the most critical sugars include sucrose, glucose, and fructose [23]. The results showed no significant difference was observed in the alcohol-soluble saccharide content of any of the green asparagus spear samples during the 20-day storage period (Table 1). This result may be due to the short storage period, which prevented the effect of different treatments on the saccharide content of green asparagus spears. Thus, it has been reported that, regardless of the treatment, fructose and glucose are rapidly depleted in asparagus (*Gijnlim*) spear tips during refrigeration, while there are no differences in either fructose or glucose content with atmospherically controlled storage [1].

Conclusions

In the active MAP system, O_2 and CO_2 mass transfer rates are the major factors controlling the speed of reagent deoxygenation and CO_2 production. Therefore, the mass transfer rate of the gas equation, which was used to simulate the rate of variation of O_2 and CO_2 concentrations in the packaging system, revealed that the theoretical value approximated the practical observation. Thus, this study successfully developed an equation model that has the potential to describe changes in O_2 and CO_2 concentrations during the storage of green asparagus spears using MAP systems. MAP reagents, green asparagus spears, and packaging film are the factors that affect changes in oxygen and carbon dioxide concentrations during storage. The results showed that the theoretical values were close to the practical observations and confirmed that the equation could be used to successfully determine the positive MAP system composition. Future studies should focus on various factors affecting the system, such as the moisture absorption rate of MAP reagents, permeability of the film by relative humidity, degree of senescence with fruits and vegetables, and respiration rate, which should be considered in the future to develop a perfect equation model. Therefore, a combination of related technologies should be considered. The equations in this study will provide valuable insights into additional economic benefits when widely applied to any fresh food with an extended shelf life to minimize post-harvest and financial losses.

Acknowledgements

The authors would like to thank the Rong Sing Medical Foundation for financial support of this project. They also thank the assistant of Ian Oktavian for the graphic abstract design of this manuscript.

Author contributions
P-HL contributed to conceptualization, investigation, writing—original draft, visualization and writing—reviewing and editing; W-CL, C-JL, and P-HL were involved in methodology, resources, and reviewing; C-JL, B-HC, and P-HL were involved in investigation and resources; W-CL and C-JL contributed to methodology and resources; B-HC and P-HL contributed to reviewing; P-HH, B-HC, and P-HL were involved in methodology, resources, and writing—reviewing and editing; P-HH, W-CL, and C-JL contributed to conceptualization, writing—reviewing and editing, supervision, and project administration; B-HC and P-HL were involved in conceptualization, resources, writing—original draft, reviewing, and editing, supervision, and project administration. All the authors read and approved the final manuscript.

Funding
This research was financially supported by the Taichung Veterans General Hospital and by the Rong Sing Medical Foundation, Taiwan. This research was also supported by Grants from the Ministry of Science and Technology (MOST 111-2313-B-126-002-) in Taiwan.

Data availability statement
Data available within the article or its supplementary materials.

Declarations

Ethics approval and consent to participate
This manuscript is an original paper that has not been published in any other journal. The authors agreed to maintain the copyright rule.

Consent for publication
The authors agree with the publication of this manuscript in this journal.

Competing interests
The authors declare that they have no conflicts of interest.

Author details
[1]Department of Food and Beverage Management, Chung-Jen Junior College of Nursing, Health Sciences and Management, Chia-Yi, Taiwan (R.O.C.). [2]Cardiovascular Center, Taichung Veterans General Hospital, Taichung, Taiwan (R.O.C.). [3]Department of Food and Nutrition, Providence University, Taichung, Taiwan (R.O.C.). [4]Institute of Food Science and Technology, National Taiwan University, Taipei, Taiwan (R.O.C.). [5]Department of Food Science and Biotechnology, National Chung Hsing University, Taichung City, Taiwan (R.O.C.). [6]School of Food, Jiangsu Food and Pharmaceutical Science College, Huai'an, Jiangsu, China.

Received: 6 October 2022 Accepted: 20 January 2023
Published online: 12 July 2023

References

1. Anastasiadi M, Collings ER, Terry LA. Investigating the role of abscisic acid and its catabolites on senescence processes in green asparagus under controlled atmosphere (CA) storage regimes. Postharvest Biol Technol. 2022;188:111892. https://doi.org/10.1016/j.postharvbio.2022.111892.
2. Baldwin SA, Van Weert G. On the catalysis of ferrous sulphate oxidation in autoclaves by nitrates and nitrites. Hydrometallurgy. 1996;42(2):209–19. https://doi.org/10.1016/0304-386X(95)00092-U.
3. Belay ZA, Caleb OJ, Opara UL. Influence of initial gas modification on physicochemical quality attributes and molecular changes in fresh and fresh-cut fruit during modified atmosphere packaging. Food Packaging Shelf Life. 2019;21:100359. https://doi.org/10.1016/j.fpsl.2019.100359.
4. Bergamasco E, Peron G, Venerando A, Ahmed Polash S, Shukla R, Sut S, Masi A. Investigation of sulfur-containing compounds in spears of green and white Asparagus officinalis through LC-MS and HS-GC–MS. Food Res Int. 2022;162:111992. https://doi.org/10.1016/j.foodres.2022.111992.
5. Bidwell GL, Walton GP. The determination of crude fiber. J Assoc Off Agric Chem. 2020;2(1):32–5. https://doi.org/10.1093/jaoac/2.1.32.
6. Boonsiriwit A, Lee M, Kim M, Itkor P, Lee YS. Exogenous melatonin reduces lignification and retains quality of green asparagus (*Asparagus officinalis* L). Foods. 2021;10(9):2111.
7. Brandenburg JS. Chapter 10 - Packaging design: Functions and materials. In: Gil MI, Beaudry R, editors. Controlled and modified atmospheres for fresh and fresh-cut produce. New York: Academic Press; 2020. p. 185–210.
8. Capobianco C. Concrete moisture meters and calcium chloride tests: there are better ways to test concrete for moisture. Floor Covering Installer. 2007;45:6.
9. Demirel Y. 1 - Fundamentals of equilibrium thermodynamics. In: Demirel Y, editor. Nonequilibrium Thermodynamics. 2nd ed. New York: Elsevier; 2007. p. 1–52.
10. Gülçin İ. Fe3+–Fe2+ Transformation Method: An Important Antioxidant Assay. In: Armstrong D, editor. Advanced Protocols in Oxidative Stress III. New York: Springer; 2015. p. 233–46.
11. Huang P-H, Cheng Y-T, Chan Y-J, Lu W-C, Li P-H. Effect of heat treatment on nutritional and chromatic properties of Mung Bean (*Vigna radiata* L). Agronomy. 2022;12(6):1365.
12. Jones AM, Griffin PJ, Collins RN, Waite TD. Ferrous iron oxidation under acidic conditions – The effect of ferric oxide surfaces. Geochimica Cosmochimica Acta. 2014;145:1–12. https://doi.org/10.1016/j.gca.2014.09.020.
13. Khamespanah F, Marx M, Crochet DB, Pokharel UR, Fronczek FR, Maverick AW, Beller M. Oxalate production via oxidation of ascorbate rather than reduction of carbon dioxide. Nat Commun. 2021;12(1):1997. https://doi.org/10.1038/s41467-021-21817-w.
14. Ku YG, Bae JH, Namieśnik J, Barasch D, Nemirovski A, Katrich E, Gorinstein S. Detection of bioactive compounds in organically and conventionally grown asparagus spears. Food Anal Methods. 2018;11(1):309–18. https://doi.org/10.1007/s12161-017-1074-0.
15. Langham WS. Determination of oxygen and carbon dioxide in medicinal gas mixtures by gas-solid chromatography. J Assoc Off Anal Chem. 2020;6:89.
16. Lee DS. Atmospheric Dynamics in MAP of Foods. In Modified Atmosphere Packaging of Foods. 2021. p. 1–444. https://doi.org/10.1002/9781119530916.ch2
17. Li L, Li C, Sun J, Xin M, Yi P, He X, Tang J. Synergistic effects of ultraviolet light irradiation and high-oxygen modified atmosphere packaging on physiological quality, microbial growth and lignification metabolism of fresh-cut carrots. Postharvest Biol Technol. 2021;173:111365. https://doi.org/10.1016/j.postharvbio.2020.111365.
18. Li T, Zhang M. Effects of modified atmosphere package (MAP) with a silicon gum film window on the quality of stored green asparagus (Asparagus officinalis L) spears. LWT Food Sci Technol. 2015;60(2):1046–53. https://doi.org/10.1016/j.lwt.2014.10.065.
19. Lin C-M, Hou C-Y, Shih M-K, Hsieh C-W, Hung Y-L, Huang P-H. Use of Incinerated Eggshells to Produce Pidan. Sustainability. 2022;14(11):6797.
20. Lwin WW, Srilaong V, Boonyaritthongchai P, Wongs-Aree C, Pongprasert N. Electrostatic atomised water particles reduces postharvest lignification and maintain asparagus quality. Sci Hortic. 2020;271:109487. https://doi.org/10.1016/j.scienta.2020.109487.
21. Mirzaei MS, Taherpour AA, Mirzaei S. Proton shuttle efficiency of bicarbonate: A theoretical study on tautomerization and CO2 hydration. Tetrahedron. 2019;75(48):130693. https://doi.org/10.1016/j.tet.2019.130693.
22. Mottern HH, Nelson EM, Walker R. The reducing value of plant juices containing vitamin c as determined by 2, 6-dichlorophenol indophenol. J Assoc Offi Agric Chemists. 2020;15(4):614–6. https://doi.org/10.1093/jaoac/15.4.614.
23. Park M-H. Sucrose delays senescence and preserves functional compounds in *Asparagus officinalis* L. Biochem Biophys Res Commun. 2016;480(2):241–7. https://doi.org/10.1016/j.bbrc.2016.10.036.
24. Pegiou E, Mumm R, Acharya P, de Vos RCH, Hall RD. Green and White Asparagus (Asparagus officinalis): A Source of Developmental. Chemical and Urinary Intrigue: Metabolites; 2019. https://doi.org/10.3390/metabo10010017.
25. Pines D, Ditkovich J, Mukra T, Miller Y, Kiefer PM, Daschakraborty S, Pines E. How Acidic Is Carbonic Acid? J Phys Chem B. 2016;120(9):2440–51. https://doi.org/10.1021/acs.jpcb.5b12428.
26. Pu Y, Zhou Q, Yu L, Li C, Dong Y, Yu N, Chen X. Longitudinal analyses of lignin deposition in green asparagus by microscopy during high

oxygen modified atmosphere packaging. Food Packaging Shelf Life. 2020;25:100536. https://doi.org/10.1016/j.fpsl.2020.100536.
27. Rajesh R, Elango L, Brindha K. Chapter 6 - Methods for Assessing the Groundwater Quality. In: Venkatramanan S, Prasanna MV, Chung SY, editors. GIS and Geostatistical Techniques for Groundwater Science. New York: Elsevier; 2019. p. 57–78.
28. Sakr EAE. Structural characterization and health benefits of a novel fructan produced by fermentation of an Asparagus sprengeri extract by Lactobacillus plantarum DMS 20174. Process Biochem. 2022;118:370–80. https://doi.org/10.1016/j.procbio.2022.05.006.
29. Schmitz KS. Chapter 5 - Thermodynamics of the Liquid State. In: Schmitz KS, editor. Physical Chemistry. New York: Elsevier; 2017. p. 203–60.
30. Sergio L, Gonnella M, Renna M, Linsalata V, Gatto MA, Boari F, Di Venere D. Biochemical traits of asparagus cultivars and quality changes in two differently coloured genotypes during cold storage. LWT. 2019;101:427–34. https://doi.org/10.1016/j.lwt.2018.11.054.
31. Serpa FS, Vidal RS, Amaral Filho JHB, Santos AF, Nascimento JF, de SennaFigueiredo CM, Franceschi E. Experimental Study on the Solubility of Carbon Dioxide in Systems Containing Ethane-1,2-diol + Water + Salt (Sodium Chloride or Calcium Carbonate). J Chem Eng Data. 2017;62(1):62–8. https://doi.org/10.1021/acs.jced.6b00381.
32. Serra-Mora P, Moliner-Martínez Y, Herráez-Hernández R, Verdú-Andrés J, Campíns-Falcó P. Simplifying iron determination with o-phenanthroline in food ashes using 2-nitrophenol as an acid-base indicator. Food Anal Methods. 2016;9(5):1150–4. https://doi.org/10.1007/s12161-015-0294-4.
33. Shen J, Griffiths PT, Campbell SJ, Utinger B, Kalberer M, Paulson SE. Ascorbate oxidation by iron, copper and reactive oxygen species: review, model development, and derivation of key rate constants. Sci Rep. 2021;11(1):7417. https://doi.org/10.1038/s41598-021-86477-8.
34. Siccama JW, Oudejans R, Zhang L, Kabel MA, Schutyser MAI. Steering the formation of cellobiose and oligosaccharides during enzymatic hydrolysis of asparagus fibre. LWT. 2022;160:113273. https://doi.org/10.1016/j.lwt.2022.113273.
35. Steel L, Liu Q, Mackay E, Maroto-Valer MM. CO2 solubility measurements in brine under reservoir conditions: A comparison of experimental and geochemical modeling methods. Greenhouse Gases Sci Technol. 2016;6(2):197–217. https://doi.org/10.1002/ghg.1590.
36. Tian Z, Zhang R, Liu Y, Xu J, Zhu X, Lei T, Li K. Hemicellulose-based nanocomposites coating delays lignification of green asparagus by introducing AKD as a hydrophobic modifier. Renewable Energy. 2021;178:1097–105. https://doi.org/10.1016/j.renene.2021.06.096.
37. Toscano S, Rizzo V, Licciardello F, Romano D, Muratore G. Packaging Solutions to Extend the Shelf Life of Green Asparagus (*Asparagus officinalis* L.) 'Vegalim.' Foods. 2021;10(2):478.
38. Viera I, RodríguezArcos R, Guillen R, Jiménez A. Asparagus cultivation co-products: from waste to chance. J Food Sci Nutr. 2020;6:100057. https://doi.org/10.24966/FSN-1076/100057.
39. Wu M-C, Jiang C-M, Huang P-H, Wu M-Y, Wang YT. Separation and utilization of pectin lyase from commercial pectic enzyme via highly methoxylated cross-linked alcohol-insoluble solid chromatography for wine methanol reduction. J Agric Food Chem. 2007;55(4):1557–62. https://doi.org/10.1021/jf062880s.
40. Xue J, Zhang X, Cheng C, Sun C, Yang S. The aroma analysis of asparagus tea processed from different parts of green asparagus (*Asparagus officinalis* L.). J Food Process Preserv. 2022;46(1):e16175. https://doi.org/10.1111/jfpp.16175.
41. Yoshida M. Fructan structure and metabolism in overwintering plants. Plants. 2021;10(5):933.
42. Yu Q, Fan L. Improving the bioactive ingredients and functions of asparagus from efficient to emerging processing technologies: A review. Food Chem. 2021;358:129903. https://doi.org/10.1016/j.foodchem.2021.129903.
43. Zhang J, Zhang F, Li D, Liu Y, Liu B, Meng X. Characterization of metabolite profiles of white and green spears of asparagus officinalis L. from Caoxian, East China. Food Res Int. 2020;128:108869. https://doi.org/10.1016/j.foodres.2019.108869.
44. Zhou Y, Chang H, Qi T. Gas–liquid two-phase flow in serpentine microchannel with different wall wettability. Chin J Chem Eng. 2017;25(7):874–81. https://doi.org/10.1016/j.cjche.2016.10.006.

Publisher's Note